Bull Mater Sci (2020) 43:277
https://doi.org/10.1007/s12034-020-02247-8

© Indian Academy of Sciences

Manganese dioxide nanoparticles: synthesis, application and challenges

SONIKA DAWADI[1], AAKASH GUPTA[2], MANITA KHATRI[1], BIPLAB BUDHATHOKI[1], GANESH LAMICHHANE[1] and NIRANJAN PARAJULI[1,*]

[1]Central Department of Chemistry, Tribhuvan University, Kirtipur, Kathmandu 44618, Nepal
[2]Department of Chemistry and Biochemistry, University of Massachusetts Dartmouth, North Dartmouth, MA 02747, USA
*Author for correspondence (nparajuli@cdctu.edu.np)

MS received 7 March 2020; accepted 22 June 2020

Abstract. In recent days, manganese oxide nanoparticles (MnO_2 NPs) have intrigued material science researches extensively due to its wide range of applications. They are widely used in energy storage devices (lithium-ion batteries, capacitors), catalysts, adsorbent, sensors and imaging, therapeutic activity, etc. Since they hold a lot of distinguished potentials, a robust protocol for cheap, stable, biocompatible and eco-friendly MnO_2 NPs is necessary. They can be categorized into different phases like α, β, δ and others. Thus, owing to their peculiar character, they could be utilized for various purposes depending on the mode of action and applications. Hence, this review has summarized conventional methods, such as hydrothermal, sol–gel, oxidation–reduction used for the generation of MnO_2 NPs. Likewise, morphological characterization by various spectroscopic techniques also outlined. It is found that the particular method of generation of MnO_2 NPs is useful for a specific phase.

Keywords. Manganese dioxide nanoparticles; hydrothermal method; sol–gel method; catalyst; adsorbent; biosensor.

1. Introduction

The advent of nanotechnology has led to the development of a new research area of this century. Nanoparticles (NPs) have developed an increasing interest in science over the last three decades. The peculiar properties of NPs are often considered a separate and intermediate state of matter between individual atoms and bulk material [1]. Nanomaterials have attracted extensive attention owing not only to their fundamental significance, but also to the potential technological applications in various fields. Materials at the nanolevel have different or improved magnetic, electric and catalytic properties than that of bulk materials. So, nanomaterials can be utilized in various fields of medicine, electrical devices, environment, etc. Manganese dioxide (MnO_2) is getting attention among researchers in the field of nanotechnology due to its low toxicity [2]. MnO_2 exists in different crystal structures, such as α-(hollandite), β-(pyrolusite), γ-(nsutite), δ-(birnessite), λ-(akhtenskite), etc.; having the same basic structure of MnO_6, linked differently [3–5]. MnO_2 NPs can be differentiated based on linkages in the structure.

Both top-down and bottom-up methods can be used for preparing MnO_2 NPs. Due to the high preparation cost and structural defects on produced NPs, the top-down approach is not widely used [6]. The bottom-up approach is preferred by most of the researchers as particles of uniform size and morphology can be obtained. The wet chemical route is used for synthesizing the MnO_2 NPs. This review is mainly focused on summarizing the widely used wet chemical methods such as hydrothermal [7], redox process [8], sol–gel method [9], thermal reflux process [10], chemical precipitation method [11] and green synthesis method [12]. Though these methods are widely used, none of them are perfect. Studies are being carried out to optimize the methods by changing reaction parameters or incorporating microwave, ultrasonic waves, etc. in the synthesis [13–15].

MnO_2 NPs are easy to prepare and have good stability due to which it has been applied in various fields. The tunnel-like α-MnO_2 has been used as an electrocatalyst for oxygen reduction and oxygen evolution in both aqueous and organic electrolytes [16]. Whereas, the layered birnessite has application as a capacitor [17]. Similarly, along with this, other forms have also been used as a catalyst and adsorbents [18–21]. They are also employed in the field of biomedicine [22–24] and the activity of MnO_2 has been enhanced by doping the nanomaterials with other metals like Ni, Ag, etc. [25].

Published online: 13 October 2020

1.1 *Structure of MnO_2 NPs*

The α-MnO_2 has a double-chained structure formed by edge-sharing of MnO_6 octahedral, where corners are joined to form (1*1) and (2*2) tunnel structures. The stability of the (2*2) tunnel size, can be maintained by doping alkali metal of large size into the tunnel structure. The β-MnO_2 NPs have a single-chain (1*1) tunnel structure formed by the edge-sharing of the MnO_6 octahedral. The (1*1) tunnel structure cannot accommodate positive ions in their structure. The γ-MnO_2 is formed by the random growth of (1*1) and (1*2) domains. δ-MnO_2 has a two-dimensional structure that contains water or other cations like Na^+ or K^+ between the two sheets. Three-dimensional structure of δ-MnO_2 having flower-like architecture with good crystallinity and order is well-known. 3D nanostructure of λ-MnO_2 is a spinel-shaped structure, in which manganese is present in the octahedral sites in the ccp oxygen framework [26]. Over the years, several nanostructured objects were investigated consisting nanosheets [27], nanotubes [28,29], nanorods [30,31], nanowires [32–34], nanoflakes [34,35], nanoflowers [36], nanourchins [37,38] and nanospheres [39]. The various morphologies of nanostructured MnO_2 materials are shown by the SEM images (figure 1) [40]. Generally, birnessite structures have been poorly defined due to low crystallinity and small size of the particle [41]. Each crystal structure of MnO_2 NPs has unique properties and different preparation routes. Various methods are being used for their production, and some methods are suitable for one crystalline structure, while some for others. One can choose different routes as per the requirements and availability (table 1).

2. Synthesis of MnO_2 NPs

2.1 *Hydrothermal process*

This method uses the concept of solubility of inorganic compounds in water at elevated temperature and pressure [2]. The process is environmentally benign, where temperature and pressure variations can be used to prepare NPs with different morphologies [42]. Wang and Li [43] prepared NPs having α- and β-phases by varying the concentration of ammonium and sulphate ions in the reaction between ammonium persulphate and manganese sulphate. Similarly, by reacting potassium permanganate and manganese sulphate proportionally under hydrothermal condition, α-, β- and δ-MnO_2 can be obtained. The molar composition of reacting species defines the morphology of the NPs without changing pH over a wide range of temperatures. Moreover, as the time is changed, maintaining a constant temperature, first δ-MnO_2 is formed, indicating the δ-MnO_2 as an intermediate stage in the formation of α-MnO_2. Cao *et al* [44] carried out the hydrothermal reaction between $MnSO_4$ and $KClO_3$ at 140–200°C for 8 h. The process resulted in α-MnO_2 nanorods at 160°C, β-MnO_2 nanorods at 200°C, and the mixture of both α and β at 180°C. The reaction between manganese sulphate and acetic acid results in α-MnO_2 at 140°C, δ-MnO_2 at 100°C and γ-MnOOH at 180°C [45]. Likewise, Deng *et al* [46] synthesized rod-like MnO_2 by hydrothermal method using $KMnO_4$ and $Mn(CH_3COO)_2$ as reagents, and the diameter obtained was about 50–60 nm.

Furthermore, particles with higher crystallinity can be prepared by increasing the reaction temperature [10]. Lan *et al* [47] prepared the α-MnO_2 particles hydrothermally by dissolving an equimolar mixture of potassium persulphate, manganese sulphate and sulphuric acid diluted with potassium sulphate at different temperatures. This process resulted in the formation of particles having intensities of diffraction peak in the order of α-60 < α-80 < α-140. Similarly, Xu *et al* [48] prepared α-MnO_2 by reacting potassium permanganate and sulphuric acid in the presence of copper at 110°C at different time intervals (6, 12 and 24 h). Closed grain spheres were obtained after 6 h, which gradually changed into nanoflower consisting of nanoflakes and nanowires. At 12 h, the interior cavity of the sphere was easily observed, and after 24 h, the sphere disappeared entirely, and the nanorod alone was seen.

Moreover, 1D layered nanobelts having tens of micrometres and with narrow size dispersion width (5–15 nm) can be prepared [49]. Such nanobelts are attained by the hydrothermal treatment of commercial manganese trioxide powder in an aqueous solution of NaOH at 170°C for 12 h–1 week. Again, β-MnO_2 (tunnel 1*1 pyrolusite) has been prepared by reacting an equimolar mixture of manganese sulphate and sodium permanganate hydrothermally at 240°C for 4 days [50]. Self-assembled 3D microstructures are obtained from the α-MnO_2 NPs by hydrothermal method, in which potassium permanganate and ferric sulphate are reacted hydrothermally at 150°C for 17 h, after the addition of sulphuric acid. Microwave-assisted hydrothermal synthesis of cobalt-doped cryptomelane MnO_2 can be carried out, for which potassium sulphate, potassium persulphate, manganese sulphate and a known amount of dopant precursor are dissolved in distilled deionized water in a quartz reaction vial fitted with a magnetic stirrer and sealed with a cap. Then, synthesis is carried out by heating in a microwave synthesizer, which is programmed to heat at 200°C for 10 min [51].

2.2 *Reduction and oxidation processes*

In this process, either reduction or oxidation of manganese occurs by various reducing and oxidizing agents. Wang *et al* [52] prepared birnessite NPs by the redox reaction between potassium permanganate and ammonium oxalate. Similarly, under hydrothermal conditions, redox reaction between ammonium persulphate and Mn(II) salt produced MnO_2

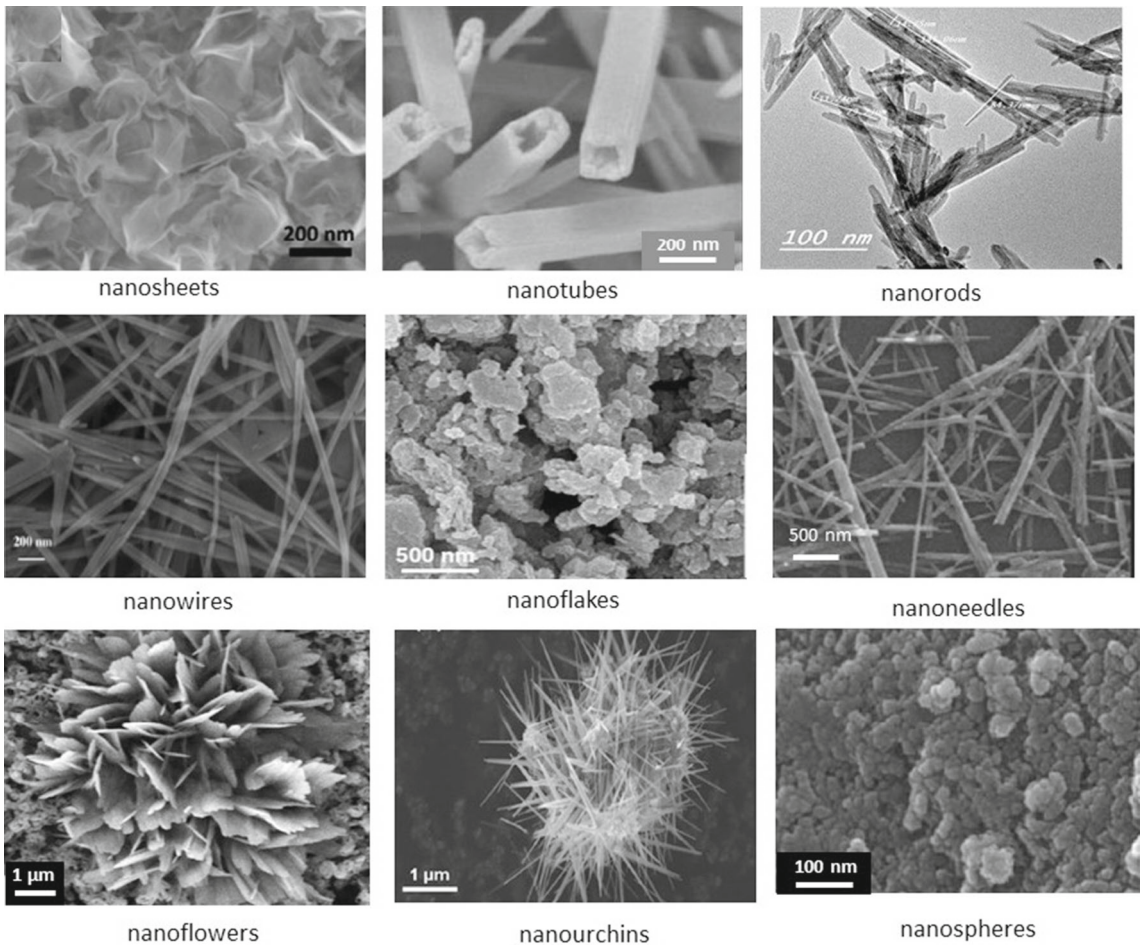

Figure 1. SEM images of the various nanostructured MnO_2 materials. Morphologies of the different MnO_2 samples are shown by the micrographs [40].

Table 1. Preparation and application of various phases of manganese dioxide NPs.

Represented nanomaterials	Methods	Applications	References
α-MnO_2, ε-MnO_2, δ-MnO_2	Hydrothermal or water bathing method	Catalyst for combustion of toluene	[2]
β-MnO_2	Reflux treatment	Catalytic degradation of methylene blue	[3]
Birnessite MnO_2	Hydrothermal	Capacitance	[4]
One-dimensional MnO_2	Quick precipitation route	Electrode	[5]
α-MnO_2, β-MnO_2	Redox	Cathode in lithium ion battery	[6]
MnO_2 and silver doped MnO_2	Green synthesis	Antibacterial activity	[7]
MnO_2 nanosheets	Redox method	Glutathione detection	[8]
β-MnO_2 nanorod	Hydrothermal	Enzymatic glucose biosensor	[9]
MnO_2 coated on zeolite	Co-precipitation	Adsorption of cephalexin	[10]
δ-MnO_2	Sol–gel process	Supercapacitors	[11]

NPs with different morphologies [53]. α-MnO_2 is obtained from manganese sulphate, and β-MnO_2 is formed from manganese nitrate. The redox reaction between MnO_4^- and Mn^{+2} is influenced by pH, temperature, oxidant, and the inorganic cations (NH_4^+ and K^+) [43]. Ragupathy *et al* [39] prepared amorphous MnO_2 of 5–15 nm size by the redox reaction between potassium permanganate and aniline. Thus, prepared amorphous MnO_2, on annealing, gives highly crystalline α-MnO_2 at 400°C. One-dimensional potassium manganese dioxide nanoribbons and nanowires

have been synthesized by the redox reaction between potassium permanganate and manganese(II) chloride in NaOH [8]. Single-layered nanosheets have been fabricated by the slow redox reaction between potassium permanganate and sodium dodecyl sulphate (SDS) [17]. SDS not only serves as the precursor of dodecanol, but also helps in the formation of nanosheets. Tang *et al* [54] synthesized the α-MnO_2 nanorods hydrothermally by the redox reaction between potassium permanganate and nitric acid.

Similarly, Li *et al* [55] mentioned the mild low temperature (60°C) reduction route for the fabrication of hollow urchin of α-MnO_2 on a large scale and potassium permanganate solution is treated with solid copper metal. δ-MnO_2 can be prepared by the oxidation of manganese(II) chloride with hydrogen peroxide in polyol medium in basic condition with microwave heating at 90°C for 10 min and ethylene glycol as the reducing agent [56–58].

2.3 *Sol–gel method*

Sol–gel is the process in which precursors of metal are hydrolysed with alcohol, water, acid, or base. In this process, the solution has to be condensed in the gel, and the remaining solvent should be removed from the system [2]. Bach *et al* [59] synthesized MnO_2 by the sol–gel route in which transparent and stable manganese oxide gel is formed by the reduction of the aqueous permanganate, $AMnO_4$ (A = K, Li, NH_4, $N(CH_3)_4$) by the fumaric acid. First of all, mixed oxides, the $AMnO_2$ are formed at a high temperature, which on oxidation with sulphuric acid leads to the formation of λ- or δ-MnO_2. Tang *et al* [60] reported the fabrication of ultrafine nanorods and nanowires by facile sol–gel method using different surfactants. In this particular method, surfactants (cetyltrimethylammonium bromide, polyvinyl pyrrolidone, etc.) were dissolved in ethanol, prior to adding manganese acetate. Nitric acid was then added to the solution. The homogeneous solution was prepared, and the prepared solution was heated in an oven at 80°C to remove the solvent. Sol–gel synthesis of sodium and potassium birnessite was also carried out [61,62]. Here, the brown gel was formed by the rapid exothermic reaction between aqueous potassium permanganate or sodium permanganate and glucose/sucrose. The formed gel was heated at 110°C for 24 h to get xerogel, which was calcined at 400–450°C for 2 h to get brown sodium and potassium birnessite NPs.

Similarly, tunnelled manganese oxide (cryptomelane) was synthesized by the reaction between aqueous $KMnO_4$ and fumaric acid in the mole ratio of 3:1 [9]. Moreover, microporous manganese oxide (birnessite, cryptomelane and spinel) can be synthesized by the non-aqueous reaction between tetrabutylammonium (TBA) or tetraethylammonium permanganate and methanol in the presence of cationic dopant. Types of the dopants and ratio of dopant and Mn are important for obtaining MnO_2 of specific morphology [63]. Oaki and Imai [64] synthesized the manganese oxide nanosheet by the complexation reaction between manganese species and ethylene diamine tetraacetate (EDTA). Here, complexation led to parallel control of reaction and morphology due to which birnessite nanosheets are produced.

2.4 *Chemical precipitation method*

In this process, NPs are formed by the controlled reaction between cation and anion. The reaction is affected by the pH, temperature and concentration of the reacting species [2]. Feng *et al* [65] studied the effect of the synthesis parameter in the formation of birnessite NPs. In the precipitation reaction between manganese(II) nitrate solution with a mixed solution of 3% H_2O_2 and sodium hydroxide, the intense peak of birnessite is obtained in the high $NaOH/Mn(NO_3)_2$ ratio, but at low concentration, β-MnOOH phase is formed. The formation is also affected by ageing and drying conditions at room temperature. One-dimensional MnO_2 is prepared by the reaction between manganese(II) chloride tetrahydrate mixed with isopropanol and the potassium permanganate solution [66]. It is found that the less amount of water resulted in the needle- or rod-like product. Whereas, a large amount of water resulted in a spindle-like product. The results have suggested that the ratio of water/isopropanol determined the morphology of the product; the different ratio leads to discordant coordination between H_2O and isopropanol with the O atom present in the unit cells of MnO_2 octahedron. Again, it is found that no MnO_2 is formed in the absence of water or the presence of isopropanol alone. Kanha and Saengkwamsawang [67] studied the effect of stirring time on the morphology and crystallinity of the MnO_2 NPs. Here, the reaction between the solution of potassium permanganate in deionized water and tris-(2-hydroxyethyl)-amine (TEA) is carried out with different stirring and calcination times at 400°C. It was found that with an increase in stirring time, crystal size and strain of α-MnO_2 are decreased, but with the increase in calcination time; crystal size and strain of α-MnO_2 are increased. It has been found that the ultrasonic-assisted co-precipitation method can be used for the self-assembly of the ultrathin MnO_2/graphene with 3-dimensional structures [68]. Shaker and Abdalsalm [11] synthesized the manganese dioxide by chemical precipitation method using inorganic precursor and toluene as a solvent with calcination temperature of 500°C.

2.5 *Reflux, thermal*

Reflux synthesis is remarkable because it produces a large number of particles. Feng *et al* [69] synthesized 3*3 tunnel-structured MnO_2 NPs by refluxing at 120°C at atmospheric pressure using birnessite NPs as a precursor (120°C). Liu *et al* [70] synthesized β-MnO_2 rods using

the reflux method. Here, the sodium hydroxide solution was added to the homogeneous solution of manganese(II) sulphate monohydrate and sodium persulphate in deionized water, and heated according to the temperature raised procedure. The diameter of nanorods ranged from 50–80 nm, and lengths ranging from 1–2 μm were obtained. A novel approach in which the polyol reflux process was used to synthesize birnessite NPs by mixing NaOH, poly(vinyl pyrrolidone), ethylene glycol and H_2O_2 and refluxing at 100°C for 1 h with magnetic stirring [39]. Zhang *et al* [13] synthesized a large scale of γ-NPs and α-NPs having an urchin-like structure within 5 min using facile microwave-assisted reflux method without using template and surfactant. Similarly, single-crystalline β-MnO_2 nanorods (diameter 20–50 nm and length 0.5–2 μm) are synthesized through the reflux treatment of potassium permanganate and manganese(II) sulphate in nitric acid solution. Again, reflux synthesis could be used in the synthesis of doped NPs [10].

In the thermal decomposition process, the chemical precursor is heated at a suitable temperature, and the waste products are removed as gas. A single-phase α-MnO_2 not having to stabilize cations in the tunnel structure has been synthesized by heating hollandaise type $(NH_4)_xMn_8O_{16}$ [71]. $K_xMnO_{2+\delta}{\cdot}nH_2O$ have been formed by the direct thermal decomposition of potassium permanganate powder. Readily available $KMnO_4$ can be decomposed at a temperature of 200–800°C, the reaction is as

$$KMnO_4 \rightarrow K_3MnO_4 + K_2MnO_4 + MnO_2 + O_2$$

Here, decomposition is considered to be reductive, and the products at 600 and 800°C are indexed δ-MnO_2 [72,73]. Similarly, Zhiliang *et al* [74] synthesized high surface area tunnel type α-MnO_2 by solvent-free heating of the homogenous mixture of $KMnO_4$ and $Mn(CH_3COOH)$ ($KMnO_4$:$Mn(CH_3COOH)$ = 2:3) in a glass bottle at 80°C for 4 h; the BET surface area of thus prepared particles is found to be 153 $m^2\ g^{-1}$.

2.6 *Green synthesis*

Green synthesis utilizes plants and microorganisms for the synthesis of NPs [75,76]. Here, plant extract acts as reducing and capping agents. Sinha *et al* [12] synthesized monodispersed orthorhombic MnO_2 using heavy metal resistance species of *Bacillus* sp. The MnO_2 synthesized were intracellular and recoverable. The process also served to remediate manganese pollution. Plants containing antioxidants like tea leaves, lemon, etc. can also be used to prepare the NPs. The antioxidant polyphenols present in the plant serve as reducing and stabilizing agents [77,78]. Similarly, a plant extract from *Kalopanaxpictus* and *Yucca gloriosa* with curcumin was used to prepare NPs of size 19.2 and 80 nm, respectively, at room temperature, without using the catalyst and other costly materials [79,80]. Again, the particle growth of α-MnO_2 can be controlled during heating by the natural capping agents [81].

3. Characterization

Different techniques can characterize NPs. Crystallographic information and purity of the phase can be obtained from the X-ray diffraction (XRD) [82]. The XRD peaks at 2θ = 12.7, 18.0, 28.6, 37.5, 41.9 and 49.7 are found for α-MnO_2 [47]. The intensity of the peak increases as the synthesis temperature and synthesis time of the NPs increases, which indicates that the crystallinity of the NPs increases with an increase in temperature and reaction time and matches with standard values.

Similarly, crystallinity can be increased by changing the ratio of reacting species [83]. Birnessite form is more crystalline than that of another phase [50]. The crystallinity of the phase does not change in introducing the pores on the surface of the NPs [84]. Furthermore, disordered components which cannot be identified by XRD can be identified by Fourier transform infrared (FTIR) spectroscopy as the metal–oxygen bond is sensitive to the IR [85]. The δ-MnO_2 shows stretching vibration in the range of 1400–1650 cm^{-1}, which indicates the existence of adsorbed and crystal water [86].

Similarly, another band at 518 cm^{-1} represents Mn–O bond vibration. Results obtained from FTIR can be confirmed by the Raman spectroscopy. It can be used to find the defects present in the NPs. Raman spectroscopy is suitable for the amorphous materials where defects are present [87]. Birnessite-type MnO_2 NPs have low Raman activity [88]. Chemical composition of the prepared NPs can be determined by the energy dispersive X-ray spectroscopy (EDX) and is used to find the composition of the materials, especially the K/Mn ratio [50,57].

Moreover, scanning and transmission electron microscopies (SEM and TEM) are used to analyse the morphology of the prepared MnO_2 NPs. It is found that temperature plays an important role in controlling the morphology of the NPs by controlling the nucleation process [47]. In low magnification mode, the structure of α-MnO_2 is 3D dandelion-like microspheres, but in high magnification mode, each microsphere is constructed of uniform radical nanorod of diameter 30 nm. By using high magnification SEM, it has been found that thin plates of α-MnO_2 gradually changes into urchin-like α-MnO_2 on increasing the reaction time. Tang *et al* [89] used SEM and found the size of K-birnessite nanobundles to be 50 μm long and 20–50 nm wide. A sheet-like morphology of δ-MnO_2 NPs is confirmed by the SEM image [90]. Rod-like, flower-like and dumbbell-like morphologies of the NPs prepared by different reactions have been confirmed by the use of SEM and TEM [91]. Morphology of the amorphous MnO_2 NPs can be known by the use of high-resolution transmission electron microscope (HRTEM) images. The HRTEM shows that amorphous

manganese dioxide NPs are with random orientation and crystallite sizes of <10 nm. Selected area electron diffraction (SAED) can be used to identify the polycrystallinity of the prepared NPs [83].

4. Applications of MnO_2 NPs

4.1 *Energy storage*

MnO_2 NPs can absorb and intercalate ions inside it. Due to this property, manganese oxides can be used as capacitors. MnO_2-based electrochemical capacitors and supercapacitors have higher power density, fast charging and discharging time, and a longer life span. Apart from good pseudocapacitance behaviour, MnO_2 nanomaterial is cheaper and environment-friendly [92]. According to Xu *et al* [48], the urchin-like α-MnO_2 has a large surface area with uniform pore distribution due to which it shows the best electrochemical capacitance. Ragupathy *et al* [39] prepared the MnO_2 electrode in which the conductivity of the MnO_2 was improved by the addition of acetylene black as the conducting materials, and the specific capacitance of 250 F g^{-1} was measured at the current density of 0.5 mA cm^{-2}. The capacitance of the MnO_2 is different for different crystallographic forms. γ-MnO_2 (311 F g^{-1}) has higher capacitance than α-MnO_2 (163 F g^{-1}) NPs [13]. Liu *et al* [17] prepared the symmetric capacitor based on the single-layered MnO_2 nanosheets having high specific capacitance and durability, retaining 91% of initial capacitance after 10,000 charges/discharge cycles. Similarly, δ-MnO_2 shows a high specific capacitance of 272 F g^{-1} and the specific capacitance retention of over 96.7% after 1000 scans [90]. Different crystallographic forms of MnO_2 NPs have a relatively equivalent series of resistance, which is helpful for the secure transport of the electrolytic ions and the electrons [93]. Similarly, the capacitance order is δ-MnO_2 > amorphous MnO_2 > α-MnO_2 > α+β-MnO_2 > β-MnO_2. The lower ratio of capacitance and performance due to less conductivity of the MnO_2 can be improved by the change in the electrolyte, and the capacitance of the MnO_2 is increased in the KI electrolyte than that in Na_2SO_4 [94].

Lithium battery systems with MnO_2 as a positive electrode can be used as a light weight battery [95]. Layered MnO_2 NPs for rechargeable lithium batteries have been prepared. It is found that a framework that is supported by potassium ions and water molecules play a vital role in determining the performance as a rechargeable battery [72]. Similarly, preparation methods affect the performance of the MnO_2 in an alkaline battery. The α-MnO_2 rod showed increased discharge property than the commercial electrolytic manganese dioxide [54]. Moreover, crystal structure also affects the performance of the electrode; excellent electrochemical performance is seen for β-MnO_2, which shows a specific discharge capacity of 180 and 130 mAh g^{-1} at first and 45th cycle, respectively, as compared to α having 210 mAh g^{-1} at first and 115 mAh g^{-1} at 45th cycle [53].

4.2 *Catalyst*

One of the significant catalytic reactions shown by the MnO_2 is in the oxidation of water, which is carried out by mimicking the natural photosystem II of the plant, which contains Mn_4O_4Ca [85]. Oxidation of water can be carried out using different crystalline structures of the MnO_2 NPs, and a water oxidation reaction depends on the crystal structures. Amorphous manganese dioxide has higher catalytic activity than that of cryptomelane type tunnel and layered birnessite-type manganese dioxide NPs [85]. Water oxidation catalytic activity of nanomanganese ferrite supported 1D (tunnelled), 2D (layered) and 3D (spinel) manganese oxide is higher than that of non-ferrite supported manganese dioxide [96].

Moreover, manganese dioxide NPs can be used in the oxidative reactions of the organic compounds, including various dyes. Crystalline tunnel-structured manganese dioxide has been used for the oxidation of propanol to acetone at room temperature photochemically [97]. The metal-doped NPs are more active photocatalysts than undoped MnO_2; doping with Fe metal on cryptomelane increases the Mn average oxidation state (AOS), coherent crystal domain (CSD) and K^+ ions in the tunnel structure, which improves the photocatalytic degradation of phenol [10]. Similarly, cryptomelane NPs prepared by the solvent-free method show higher catalytic activity for the oxidation of alcohol than prepared by conventional methods. It is due to the higher surface area and novel surface properties [98]. Again, a mesoporous α-MnO_2 nanorod having a small size of 40 nm is prepared at 40°C and has a higher activity for toluene combustion than that having larger size prepared at the higher temperature (60 and 80°C) [4]. Transition metal-doped cryptomelane type NPs (Ce) are used for the oxidation of ozone in the atmosphere containing waste gases [99]. MnO_2 is used in the Fenton type reactions for the catalytic degradation of dyes. β-nanorod of a diameter 20–50 nm and a length of 0.5–2 μm is used to degrade methylene blue dye in the presence of H_2O_2 [31]. In the same way, α-MnO_2 nanowires having a high surface area are used for the degradation of the azo dye; about 70% dyes were removed within 20 min using 20 mg MnO_2 nanowires [100]. The porous nature of manganese dioxide has been used for the degradation of malachite green in aqueous solution under ambient conditions [101].

4.3 *Electrochemical materials*

Manganese dioxide NPs are also used as an oxygen reducing electrode in fuel cells. The oxygen reduction capacity can be increased by preparing manganese dioxide

having higher defects or high conductivity. The α-MnO_2 prepared at 80°C with moderate defects, and electrical conductivity showed more significant oxygen reduction catalytic activity [47]. The presence of a cationic dopant increases the electron-donating ability of the manganese dioxide NPs. The activity of Ni-α-MnO_2 and Cu-α-MnO_2 have a higher oxygen reduction capacity than that of undoped manganese dioxide [102].

Similarly, oxygen reduction activity also depends on the crystalline structure of the NPs. Meng *et al* [50] found that α-MnO_2 NPs have higher oxygen reducing properties. Order of activity is the most potent oxygen absorption ability of α-MnO_2.

4.4 *Adsorbent*

Manganese dioxide NPs are found in the form of octahedral molecular sieves of large surface area due to which they are used in the adsorption of heavy metals and organic pollutants from water [103]. To improve the adsorption, manganese dioxide nanomaterials are combined with magnetic compounds that provide efficient wastewater treatment in the presence of the external magnetic field [104,105]. MnO_2 NPs have recently been commonly used for dye removal due to the effect of chemical and physical interactions between organic (polymer) and inorganic (MnO_2 NPs) materials [106,107]. The super magnetic NPs exhibit high saturation magnetization, which makes the separation procedure convenient at room temperature [108]. Again, manganese dioxide NPs can be placed in other metal oxides to improve the activity of the metal oxide. Dai *et al* [109] prepared the hierarchical K-birnessite nanoplates on anatase nanofibres and used the prepared NPs for the removal of congo red from an aqueous solution, which shows good activity in both continuous and batch flow studies. γ-Fe_2O_3 and α-MnO_2 can be incorporated onto the ball-mill expanded Perlite carrier materials, which are used for the successful removal of the arsenic metal from the water. γ-MnO_2/α-MnO_2 core/shell materials are used for water treatment and show the excellent property for the removal of organic and heavy metal pollution [110]. Similarly, manganese dioxide NPs can trap the pollutants in the interlayer gaps of layered NPs; aniline is trapped in the interlayer [111].

4.5 *Biomedical applications*

Manganese dioxide acts as a bi-directional electrocatalytic for the oxidation and reduction of H_2O_2 [112]. Using this property, choline biosensor has been prepared by electrochemical deposition of bio-composite made up of chitosan hydrogel, choline oxidase and MnO_2 NPs onto glassy carbon electrode [113]. Hierarchical MnO_2 microsphere composed of nanodisk electrodes are synthesized for sensing the nitrite, due to high surface area and conductivity, the electrode shows high catalytic activity and much low detection limit for nitrite sensing [114]. The study has been done to know the effect of interference ions (glucose, uric acid and ascorbic acid) on nitrite sensitivity. Moreover, it is found that nitrite sensitivity is not affected by interference ions as they are oxidized in basic pH, not in neutral pH, which is used in the study [115]. MnO_2 nanorods have been found to sense potassium ions as well [116]. MnO_2 NPs are used in non-enzymatic H_2O_2 sensors, thiol sensors, xenoestrogens detection, glutathione detection, etc. [85–88].

Manganese dioxide NPs and their composites have been used in medical research. It can be used as antibacterial and antifungal agents. The nanocomposite is found to be more effective against both Gram-positive and Gram-negative bacteria [117,118]. Similarly, MnO_2/black cumin composite is used as antibacterial agents in water [24]. MnO_2 NPs have potential applications in magnetic resonance imaging and targeted drug delivery [119]. The high reactivity of MnO_2 NPs with the cellular hydrogen peroxide has been utilized to alleviate cellular hypoxia in cancer treatment [120,121]. Manganese oxide-based catalytic tubular micrometer produced by template electrodeposition method can perform self-propelling therapeutics devices that can deliver anticancer drugs [122].

5. Challenges

Manganese dioxide NPs have been synthesized by different methods, but there are still challenges for obtaining the required NPs. While preparing NPs by hydrothermal method, temperature and reaction time need to be considered, as with changes in the parameters, phase and morphology of the particles change. At relatively low-temperature, fine particles are formed, which aggregates at high temperatures to give coarse crystalline materials [98]. Similarly, the surface area also decreases with an increase in the crystallinity of the particles. The ageing process in both room temperature and hydrothermal synthesis affects the structure of the final products. Undisturbed ageing treatment is essential to obtain crystalline particles [65].

Similarly, reaction times play a crucial role in the preparation of different phases, and it has been found that at lower reaction time, birnessite can be prepared, and long reaction time should be avoided if the particles with the high surface area are required [48]. Moreover, the solvent system also affects the structure of the particles as the small amount of water gives nanorods and nanowires, but a higher amount of water gives spindle-shaped NPs [66]. When preparing MnO_2 NPs, care must be taken about the amount of reacting species. With increasing the ratio of $KMnO_4$/$(NH_4)_2C_2O_4$ produces the compact NPs [15]. The production of α-MnO_2 and γ-MnO_2 by the oxidation of Mn^{2+} in acidic condition; α-MnO_2 was produced in the presence of H_2SO_4 and γ-MnO_2 was produced in the presence of HNO_3

and HCl from which it is clear that pH needs to be balanced to obtain the particular crystal structures [95]. It is also crucial to choose effective reducing agents for the preparation of MnO_2 NPs. Yang *et al* [56] found that ethylene glycol is an effective reducing agent for the synthesis of potassium birnessite NPs. Again, care must be given in the concentration of the reacting materials as the highly concentrated mixture produces layered, but the less concentrated produces cryptomelane and Mn_2O_3 NPs [9]. Similarly, different surfactants have different effects on the preparation of NPs. Cetyl trimethyl ammonium bromide (CTAB) helped in the formation of highly dispersed NPs, while polyvinyl pyrrolidone (PVP) gave the aggregated NPs [60].

6. Conclusions

MnO_2 NPs have a wide range of applications ranging from electrochemical applications, sensors, biomedical, etc. They exhibit varied structures and morphologies, which can mainly be distinguished based on MnO_6 linkage. The hydrothermal method is the right approach for the generation of MnO_2 NPs due to its ease of operation, morphology, crystal structure and other properties. Green synthesis has emerged as a potential alternative to chemical methods and is cheaper and environment-friendly. They have also shown to exhibit catalytic activities. Treatment of MnO_2 NPs with multidrug-resistant bacterial and cancer therapies is an area of prime concern for further research. Manganese dioxide nanocomposites are found to be effective against bacteria and can be used to target drug delivery against cancer due to its ability of functionalization. However, all the synthesized NPs are applied in the laboratory conditions only; more research is needed for the practical and product-oriented application of the NPs. So, extensive research needs to be carried out for the application of MnO_2 NPs in these areas. The effect of NPs on the ecosystem needs to be adequately studied, although it is considered environment-friendly.

References

[1] Schmid G 2006 *Nanoparticles: from theory to applications* 2nd edn (Wiley-VCH)
[2] Burda C, Chen X, Narayanan R and El-Sayed M A 2005 *Chem. Rev.* **105** 1025
[3] Najafpour M M and Allakhverdiev S I 2012 *Int. J. Hydrog. Energy* **37** 8753
[4] Lin T, Yu L, Sun M, Cheng G, Lan B and Fu Z 2016 *Chem. Eng. J.* **286** 114
[5] Štengl V, Králová D, Opluštil F and Němec T 2012 *Micropor. Mesopor. Mater.* **156** 224
[6] Nikam A V, Prasad B L V and Kulkarni A A 2018 *CrystEngComm* **20** 5091
[7] Qi S Y, Feng J, Yan J, Hou X Y and Zhang M L 2008 *Chin. J. Nonferrous Met.* **18** 113
[8] Zhang H T, Chen X H, Zhang J H, Wang G Y, Zhang S Y, Long Y Z *et al* 2005 *J. Cryst. Growth* **280** 292
[9] Ching S, Roark J L, Duan N and Suib S L 1997 *Chem. Mater.* **9** 750
[10] Yin H, Dai X, Zhu M, Li F, Feng X and Liu F 2015 *J. Hazard. Mater.* **296** 221
[11] Shaker K and Abdalsalm A H 2018 *Eng. Tech. J.* **36** 946
[12] Sinha A, Nand V, Raj B and Kumar S 2011 *J. Hazard. Mater.* **192** 620
[13] Zhang X, Sun X, Zhang H, Zhang D and Ma Y 2013 *Electrochim. Acta* **87** 637
[14] Ai Z, Zhang L, Kong F, Liu H, Xing W and Qiu J 2008 *Mater. Chem. Phys.* **111** 162
[15] Abulizi A, Yang G H, Okitsu K and Zhu J J 2014 *Ultrason. Sonochem.* **21** 51629
[16] Benbow E M, Kelly S P, Zhao L, Reutenauer J W and Suib S L 2011 *J. Phys. Chem. C* **115** 22009
[17] Liu Z, Xu K, Sun H and Yin S 2015 *Small* **11** 20182
[18] Robinson D M, Go Y B, Mui M, Gardner G, Zhang Z, Mastrogiovanni D *et al* 2013 *J. Am. Chem. Soc.* **135** 93494
[19] Chakrabarti S, Dutta B K and Apak R 2009 *Water Sci. Technol.* **60** 3017
[20] Liao X, Zhang C, Liu Y, Luo Y, Wu S, Yuan S *et al* 2016 *Chemosphere* **150** 90
[21] Shaban M, Abukhadra M R, Ibrahim S S and Shahien M G 2017 *Appl. Water Sci.* **7** 4743
[22] Sivaraj D and Vijayalakshmi K 2017 *Mater. Sci. Eng.* **81** 469
[23] Krishnaraj C, Ji B J, Harper S L and Yun S I 2016 *Biopro. Biosyst. Eng.* **39** 759
[24] Siddiqui S I, Manzoor O, Mohsin M and Chaudhry S A 2018 *Environ. Res.* **171** 32018
[25] Dong J, Hou Z, Zhao Q and Yang Q 2019 *E3S Web. Conf.* **03002** 1
[26] Julien C, Mauger A, Vijh A and Zaghib K (eds) 2016 *Lithium batteries: science and technology* (Switzerland: Springer)
[27] Zhai L, Wang W, Yu C, Wang P and Mao Y 2014 *Anal. Chem.* **86** 12206
[28] Luo J, Zhu H T, Fan H M, Liang J K, Shi H L, Rao G H *et al* 2008 *J. Phys. Chem.* **112** 12594
[29] Zheng X, Sun D, Fan S, Yu W, Fan H, Cao C *et al* 2005 *J. Phys. Chem.* **109** 16439
[30] Sugantha M, Ramakrishnan P A, Hermann A M and Ginley D S 2003 *Int. J. Hydrog. Energy* **28** 597
[31] Cui H J, Huang H Z, Fu M L, Yuan B L and Pearl W 2011 *Catal. Commun.* **12** 1339
[32] Wang X and Li Y 2002 *J. Am. Chem. Soc.* **124** 2880
[33] Wei M, Konishi Y, Zhou H, Sugihara H and Arakawa H 2005 *Nanotechnology* **16** 245
[34] Yuan Z Y, Ren T Z, Du G H and Su B L 2005 *Appl. Phys. A: Mater. Sci. Process.* **804** 743
[35] Sun P, Yi H, Peng T, Jing Y, Wang R, Wang H *et al* 2017 *J. Power Sources* **341** 27
[36] Jana S, Pande S, Sinha A K, Sarkar S, Pradhan M, Basu M *et al* 2009 *J. Phys. Chem.* **1134** 1386
[37] Hashem A M, Abdel-Ghany A E, El-Tawil R, Bhaskar A, Hunzinger B, Ehrenberg H *et al* 2016 *Ionics* **22** 2263

[38] Song X C, Zhao Y and Zheng Y F 2007 *Cryst. Growth Des.* **7** 159
[39] Ragupathy P, Vasan H N and Munichandraiah N 2007 *J. Electrochem. Soc.* **155** 34
[40] Julien C M and Mauger A 2017 *Nanomaterials* **711** 1
[41] Brock S L, Duan N, Tian Z R, Giraldo O, Zhou H and Suib S L 1998 *Chem. Mater.* **10** 2619
[42] Byrappa K and Adschiri T 2007 *Prog. Cryst. Growth Charact. Mater.* **53** 117
[43] Wang X and Li Y 2003 *Chem. Eur. J.* **9** 300
[44] Cao G, Su L, Zhang X and Li H 2010 *Mater. Res. Bull.* **45** 425
[45] Cheng G, Yu L, Lan B, Sun M, Lin T, Fu Z *et al* 2016 *Mater. Res. Bull.* **75** 17
[46] Deng J M G, Feng Y H, Fang Q and Chen Y F 2009 *Funct. Mater. Dev.* **15** 503
[47] Lan B, Zheng X, Cheng G, Han J, Li W, Sun M *et al* 2018 *Eletcrochim. Acta* **283** 459
[48] Xu M, Kong L, Zhou W and Li H 2007 *J. Phys. Chem.* **111** 9141
[49] Ma R, Bando Y, Zhang L and Sasaki T 2004 *Adv. Mater.* **16** 918
[50] Meng Y, Song W, Huang H, Ren Z, Chen S Y and Suib S L 2014 *J. Am. Chem. Soc.* **136** 11452
[51] Pahalagedara L R, Dharmarathna S, King'ondu C K, Pahalagedara M N, Meng Y T, Kuo C H *et al* 2014 *J. Phys. Chem.* **118** 20363
[52] Wang J, Li J, Jiang C, Zhou P, Zhang P and Yu J 2017 *Appl. Catal. B: Environ.* **204** 147
[53] Hashem A M, Abuzeid H M, Abdel-Latif A M, Abbas H M, Ehrenberg H, Indris S *et al* 2013 *ECS Trans.* **50** 125
[54] Tang N, Tian X, Yang C, Pi Z and Han Q 2010 *J. Phys. Chem. Solids* **71** 258
[55] Li B, Rong G, Xie Y, Huang L and Feng C 2006 *Inorg. Chem.* **45** 6404
[56] Yang L, Zhu Y and Cheng G 2007 *Mater. Res. Bull.* **42** 159
[57] Kaabi N, Chouchene B, Mabrouk W, Matoussi F, Selmane E and Hmida B H 2018 *Solid State Ion.* **325** 74
[58] Selvakumar S, Nuns N, Trentesaux M, Batra V S, Giraudon J M and Lamonier J F 2018 *Appl. Catal. B: Environ.* **223** 192
[59] Bach S, Henry M, Baffier N and Livage J 1990 *J. Solid State Chem.* **88** 325
[60] Tang W, Shan X, Li S, Liu H, Wu X and Chen Y 2014 *Mater. Lett.* **132** 317
[61] Ching S, Petrovay D J, Jorgensen M L and Suib S L 1997 *Inorg. Chem.* **36** 883
[62] Ching S, Landrigan J A, Jorgensen M L, Duan N and Suib S L 1995 *Chem. Mater.* **7** 1604
[63] Ching S, Welch E J, Hughes S M, Bahadoor A B F and Suib S L 2002 *J. Nanomater.* **8** 1292
[64] Oaki Y and Imai H 2007 *Angew. Chem. Int. Ed.* **46** 4951
[65] Feng Q, Liu L and Yanagisawa K 2000 *J. Mater. Sci. Lett.* **19** 1567
[66] Chen S, Zhu J, Han Q, Zheng Z, Yang Y and Wang X 2009 *Cryst. Growth Des.* **9** 4356
[67] Kanha P and Saengkwamsawang P 2017 *Inorg. Nano-Met. Chem.* **1** 556
[68] Zhao B, Lu M, Wang Z, Jiao Z, Hu P, Gao Q *et al* 2016 *J. Alloys Compd.* **663** 180
[69] Feng X H, Tan W F, Liu F, Wang J B and Ruan H D 2004 *Chem. Mater.* **16** 4330
[70] Liu X, Fu S and Huang C 2005 *Power. Tech.* **154** 120
[71] Muraoka Y 1999 *J. Solid State Chem.* **144** 136
[72] Komaba S, Kumagai N and Chiba S 2000 *Electrochim. Acta* **461** 31
[73] Gaillot A C, Flot D, Drits V A, Manceau A, Burghammer M and Lanson B 2003 *Chem. Mater.* **15** 4666
[74] Zhiliang J, Vinod X and Jaekook M 2016 *Chem. Phys. Lett.* **650** 64
[75] Devatha C P and Thalla A K 2018 *Micro and nano technologies* (Woodhead Publishing) p 169
[76] Hoseinpour V and Ghaemi N 2018 *J. Photochem. Photobiol. B: Biol.* **189** 234
[77] Abuzeid H M, Hashem A M, Kaus M, Knapp M, Indris S, Ehrenberg H *et al* 2018 *J. Alloys Compd.* **746** 227
[78] Hashem A M, Abuzeid H, Kaus M, Indris S, Ehrenberg H, Mauger A *et al* 2018 *Electrochim. Acta* **262** 74
[79] Hoseinpour V, Souri M and Ghaemi N 2018 *Micro Nano Lett.* **13** 1560
[80] Moon S A, Salunke B K, Alkotaini B, Sathiyamoorthi E and Kim B S 2015 *IET Nanobiotechnol* **9** 220
[81] Sanchez-Botero L, Herrera P A and Hinestroza P J 2017 *Nanomaterials* **7** 117
[82] Wang X and Li Y 2002 *J. Am. Chem. Soc.* **124** 2880
[83] Zhou J, Yu L, Sun M, Yang S, Ye F, He J *et al* 2013 *Ind. Eng. Chem. Res.* **52** 9586
[84] Wang J, Zhang G and Zhang P 2017 *J. Mater. Chem.* **5** 5719
[85] Iyer A, Dutta P and Suib S 2012 *J. Phys. Chem. C* **11** 6474
[86] Chen X, Yan S, Wang N, Peng S, Wang C, Hong Q *et al* 2017 *RSC Adv.* **7** 55734
[87] Julien C, Massot M, Rangan S, Lemal M and Guyomard D 2002 *J. Raman Spectrosc.* **33** 223
[88] Julien C, Massot M, Baddour-Hadjean R, Franger S, Bach S and Pereira-Ramos J P 2003 *Solid State Ion.* **159** 345
[89] Tang X, Li H, Liu Z, Yang Z and Wang Z 2011 *J. Power Sources* **96** 855
[90] Jia Z, Wang J, Wang Y, Li B, Wang B, Qi T *et al* 2016 *J. Mater. Sci. Technol.* **32** 147
[91] Shi F, Wang F, Dai H, Dai J, Deng J, Liu Y *et al* 2012 *Appl. Catal. A: Gen.* **433** 206
[92] Zhang Y, Feng H, Wu X, Wang L, Zhang A, Xia T *et al* 2009 *Int. J. Hydrog. Energy* **34** 4889
[93] Zhao X, Hou Y, Wang Y, Yang L, Zhu L, Cao R *et al* 2017 *RSC Adv.* **7** 40286
[94] Jiang Y, Cui X, Zu L, Hu Z, Gan J, Lian H *et al* 2015 *Nanomaterials* **5** 1638
[95] Denholm P, Ela E, Kirby B and Milligan M 2010 *Nat. Ren. En. Lab. Tech. Rep.* 25
[96] Elmaci G, Frey C E, Kurz P and Zümreoğlu-Karan B 2016 *J. Mater. Chem.* **22** 8812
[97] Iyer A, Galindo H, Sithambaram S, King'ondu C, Chen C H and Suib S L 2010 *Appl. Catal. A: Gen.* **375** 295
[98] Ding Y, Shen X, Sithambaram S, Gomez S, Kumar R, Crisostomo V M B *et al* 2005 *Chem. Mater.* **1** 5382
[99] Ma J, Wang C and He H 2017 *Appl. Catal. B: Environ.* **201** 503
[100] Ramesh M, Nagaraja H S, Rao M P, Anandan S and Huang N M 2016 *Mater. Lett.* **172** 85
[101] Saha S and Pal A 2014 *Sep. Purif. Technol.* **134** 26

[102] Lambert T N, Vigil J A, White S E, Delker C J, Davis D J, Kelly M *et al* 2017 *J. Phys. Chem. C* **121** 2789
[103] Hua M, Zhang S, Pan B, Zhang W, Lv L and Zhang Q 2012 *J. Hazard. Mater.* **211** 317
[104] Chen H, Chu P K, He J, Hu T and Yang M 2011 *J. Colloid Interf. Sci.* **359** 68
[105] Tan L, Wang J, Liu Q, Sun Y, Jing X, Liu L *et al* 2015 *J. Chem.* **39** 868
[106] Le T H, Ngo T H A, Doan V T, Nguyen L M T and Le M C 2019 *J. Chem.,* Article ID 1602752
[107] Romero P G and Sanchezb C 2005 *New J. Chem.* **29** 57
[108] Zhai Y, Zhai J, Zhou M and Dong S 2009 *J. Mater. Chem.* **19** 7030
[109] Dai Y, Lu X, McKiernan M, Lee E P, Sun Y and Xia Y 2010 *J. Mater. Chem.* **20** 3157
[110] Cao J, Mao Q, Shi L and Qian Y 2011 *J. Mater. Chem.* **21** 16210
[111] Xiao W, Zhou P, Mao X and Wang D 2015 *J. Mater. Chem. A* **3** 8676
[112] Bai Y H, Du Y, Xu J J and Chen H Y 2007 *Electrochem. Commun.* **910** 2611
[113] Dontsova E A, Zeifman Y S, Budashov I A, Eremenko A V, Kalnov S L and Kurochkin I N 2011 *Sens. Actuators* **1591** 261
[114] Xia C, Ning W and Lin G 2009 *Sens. Actuators B Chem.* **137** 710
[115] Dai Y, Huang J, Zhang H and Liu C C 2018 *Sens. Actuators B Chem.* **281** 746
[116] Ahn M S, Ahmad R, Yoo J Y and Hahn Y B 2018 *J. Colloid Interf. Sci.* **516** 364
[117] Sivaraj D and Vijayalakshmi K 2017 *Mater. Sci. Eng. C* **81** 469
[118] Krishnaraj C, Ji B J, Harper S L and Yun S I 2016 *Bioproc. Biosyst. Eng.* **39** 5759
[119] Shin J, Anisur R M, Ko M K, Im G H, Lee J H and Lee I S 2009 *Angew. Chem. Int. Ed.* **48** 321
[120] Tian L, Chen Q, Yi X, Chen J, Liang C, Chao Y *et al* 2017 *Small* **13**
[121] Song M, Liu T, Shi C, Zhang X and Chen X 2016 *ACS Nano* **10** 633
[122] Wang L, Chen J, Feng X, Zeng W, Liu R, Lin X *et al* 2016 *RSC Adv.* **6** 65624